

8-1-2018

Force Multiplier Calculations for X-ray Binaries and Active Galactic Nuclei

Randall Cody Dannen
rcdannen@gmail.com

Follow this and additional works at: <https://digitalscholarship.unlv.edu/thesesdissertations>



Part of the [Astrophysics and Astronomy Commons](#)

Repository Citation

Dannen, Randall Cody, "Force Multiplier Calculations for X-ray Binaries and Active Galactic Nuclei" (2018). *UNLV Theses, Dissertations, Professional Papers, and Capstones*. 3354.
<https://digitalscholarship.unlv.edu/thesesdissertations/3354>

This Thesis is protected by copyright and/or related rights. It has been brought to you by Digital Scholarship@UNLV with permission from the rights-holder(s). You are free to use this Thesis in any way that is permitted by the copyright and related rights legislation that applies to your use. For other uses you need to obtain permission from the rights-holder(s) directly, unless additional rights are indicated by a Creative Commons license in the record and/or on the work itself.

This Thesis has been accepted for inclusion in UNLV Theses, Dissertations, Professional Papers, and Capstones by an authorized administrator of Digital Scholarship@UNLV. For more information, please contact digitalscholarship@unlv.edu.

FORCE MULTIPLIER CALCULATIONS FOR X-RAY BINARIES AND
ACTIVE GALACTIC NUCLEI

by

Randall Cody Dannen

Bachelor of Science - Physics
Bachelor of Science - Mathematics
University of Nevada, Las Vegas
May 2016

A thesis submitted in partial fulfillment of
the requirements for the

Master of Science - Astronomy

Department of Physics & Astronomy
College of Sciences
The Graduate College

University of Nevada, Las Vegas
August 2018

Copyright by Randall Cody Damm 2018
All Rights Reserved



Thesis Approval

The Graduate College
The University of Nevada, Las Vegas

July 31, 2018

This thesis prepared by

Randall Cody Dannen

entitled

Force Multiplier Calculations for X-ray Binaries and Active Galactic Nuclei

is approved in partial fulfillment of the requirements for the degree of

Master of Science - Astronomy
Department of Physics & Astronomy

Daniel Proga, Ph.D.
Examination Committee Chair

Kathryn Hausbeck Korgan, Ph.D.
Graduate College Interim Dean

Zhaohuan Zhu, Ph.D.
Examination Committee Member

Stephen Lepp, Ph.D.
Examination Committee Member

Evangelos Yfantis, Ph.D.
Graduate College Faculty Representative

ABSTRACT

FORCE MULTIPLIER CALCULATIONS FOR X-RAY BINARIES AND ACTIVE GALACTIC NUCLEI

by

Randall Cody Dannen

Dr. Daniel Proga, Examination Committee Chair
Professor of Physics & Astronomy
University of Nevada, Las Vegas

Motivated by the work done to explore the winds from hot stars (Lamers & Cassinelli 1999), we develop a method for self consistently calculating force multipliers for Type 1 and Type 2 active galactic nuclei (AGN), soft and hard start X-ray binaries (XRBs) spectral energy distributions (SEDs). We find that the amplification to the radiation force can be as large as 100 even when the gas is highly ionized due to Fe and O ions. We discuss future efforts to incorporate these findings in magnetohydrodynamic simulations.

ACKNOWLEDGMENTS

A special thank you to my thesis Dr. Daniel Proga for his patients and expertise while working on this project. Thanks to Dr. Sergei Dyda and Dr. Tim Waters helping develop solutions to my myriad of problems, and many thanks to Tim Kallman for providing the initial version of the force multiplier code we used to calculate the force multipliers, feedback on our results, and developing XSTAR.

TABLE OF CONTENTS

ABSTRACT	iii
ACKNOWLEDGEMENTS	iv
LIST OF TABLES	vi
LIST OF FIGURES	viii
CHAPTER 1: INTRODUCTION	1
1.1 BASIC PHYSICS	1
1.2 SOBOLEV APPROXIMATION	2
1.3 THE FORCE MULTIPLIER	2
CHAPTER 2: METHODS	5
2.1 ATOMIC DATA	5
2.2 IONIZATION STRUCTURE	5
2.3 CALCULATING THE FORCE MULTIPLIER	5
CHAPTER 3: RESULTS	12
CHAPTER 4: CONCLUSION, DISCUSSION, & FUTURE WORK	29
APPENDIX: MHD BASICS	31
BIBLIOGRAPHY	32
CURRICULUM VITAE	33

LIST OF TABLES

Table 3.1: Table showing the top five contributors to the force multiplier for AGN1 with $t = 10^{-6}$ for various values of ξ . The left column for each block indicates the ion the line belongs, then its wavelength in angstroms, and then the value force multiplier for just that line $M_L(t, \xi)$	25
Table 3.2: Same as Table 3.1 but for AGN2.	26
Table 3.3: Same as Table 3.1 but for c6.	27
Table 3.4: Same as Table 3.1 but for c7.	28

LIST OF FIGURES

Figure 1.1: Simplified depiction of the momentum transfer by the absorption and emission of a photon.	1
Figure 2.1: Shown here is the distribution of the entries in our atomic datasets. Kurucz’s shown in red, XSTAR’s shown in blue, and the total list after they were carefully merged shown in black.	6
Figure 2.2: The top panels show the SEDs AGN1, AGN2 (left), c6, and c7 (right) with the flux in arbitrary units. The bottom panels shows what fraction of the total energy is in each energy band (IR, optical, UV, X-ray, and range integrated for our definition of ξ in red, green, purple, dark blue-grey, and orange respectively).	7
Figure 2.3: Shown here is are relative ion abundances for determined by XSTAR for AGN1.	8
Figure 2.4: Same as Figure 2.3 but for AGN2.	9
Figure 2.5: Same as Figure 2.3 but for c6.	10
Figure 2.6: Same as Figure 2.3 but for c7.	11
Figure 3.1: Shown is the force multiplier $M(t, \xi)$ for our four SEDs, labeled in the top right of each panel. The x-axis is our optical depth parameter t , and the lines indicate differences $\Delta \log \xi = 1$, stepping from -2 to 5, dashed for negative value, solid for positive. The color is to give some indication relative value, going from low (blue) to high (red). . . .	13
Figure 3.2: Shown is the force multiplier $M(t, \xi)$ for our four SEDs, labeled in the top right of each panel. The x-axis is our photoionization parameter ξ , and the lines indicate differences $\Delta \log t = 1$, stepping from -8 to 2, dashed for negative values, solid for positive. The color is to give some indication relative value, going from low (blue) to high (red).	14
Figure 3.3: The left panels correspond to AGN1 and the right panels correspond to AGN2. The solid black line is the thermal equilibrium curve determined by XSTAR corresponding to the right y-axis. The solid blue, dashed red, and dash-dotted green line correspond to the total force multiplier, UV component of the force multiplier, and X-ray component of the force multiplier respectively. The shaded region in the top two figures indicates where we’d expect the gas to become thermally unstable using the condition $\partial \ln T / \partial \ln \xi > 1$ (Field 1965). The bottom show η_{\max} for all lines, UV lines, and X-ray lines in solid blue, dashed red, and dash-dotted green respectively.	15
Figure 3.4: The left panels correspond to c6 and the right panels correspond to c7. The solid black line is the thermal equilibrium curve determined by XSTAR corresponding to the right y-axis. The solid blue, dashed red, and dash-dotted green line correspond to the total force multiplier, UV component of the force multiplier, and X-ray component of the force multiplier respectively. The shaded region in the top two figures indicates where we’d expect the gas to become thermally unstable using the condition $\partial \ln T / \partial \ln \xi > 1$ (Field 1965). The bottom show η_{\max} for all lines, UV lines, and X-ray lines in solid blue, dashed red, and dash-dotted green respectively.	16
Figure 3.5: We present details about the force multiplier due to individual elements for SED AGN1. We show only elements that contribute at least 10% of the total force multiplier for any value of ξ	17

Figure 3.6: We present details about the force multiplier due to individual ions for SED AGN1. We show only ions that contribute at least 10% of the total force multiplier for any value of ξ	18
Figure 3.7: Same as Figure 3.5 but for AGN2.	19
Figure 3.8: Same as Figure 3.6 but for AGN2.	20
Figure 3.9: Same as Figure 3.5 but for c6.	21
Figure 3.10: Same as Figure 3.6 but for c6.	22
Figure 3.11: Same as Figure 3.5 but for c7.	23
Figure 3.12: Same as Figure 3.6 but for c7.	24
Figure 4.1: Preliminary results from ATHENA++ using both the heating and cooling model described in Dyda et al. (2017) and force multiplier values shown in Chapter 3. Models run-01 and run-02 correspond to wind from a central object with $M = 1M_{\odot}$ and $M = 10M_{\odot}$ for run-03. $\rho_0 = 1.30 \times 10^{-13}$ run-01 and run-02, and $\rho_0 = 3.27 \times 10^{-21}$ for run-03. R_{IN} is 4.60×10^{12} cm for run-01, 1.46×10^{12} cm for run-02, and 2.91×10^{20} cm for run-03. More detailed results will be shown in Dannen & Proga (2018, in prep.)	30

CHAPTER 1: INTRODUCTION

We hope to show that line driving can be an efficient mechanism for driving winds from active galactic nuclei (AGN) and help explain the presents of extreme Doppler shifts found in the broad adsorption line line region and inform our understanding on the efficiency of line driving in X-ray binary (XRB) systems. This document will consist of the four parts. Chapter 1 will be an over view of the basic physics and the background of this problem. Chapter 2 will discuss how we calculated our values for the force multipliers. Chapter 3 will present our results, and Chapter 4 will discuss our main conclusions and future work.

1.1 BASIC PHYSICS

The change in momentum for an atom absorbing photon moving radially can be expressed as

$$mv'_r = mv_r + \frac{h\nu}{c}, \quad (1.1)$$

where m is the mass of a given atom, h is Plank's constant, c the speed of light, ν is the frequency of the absorbed photon, v_r the atoms initial velocity parallel to the absorbed photon, and v'_r is the atom's velocity after absorbing the photon. After absorbing the photon, the atom may emit a photon, then the total change in the momentum in the radial direction is

$$mv''_r = mv'_r + \frac{h\nu'}{c} \cos \alpha, \quad (1.2)$$

where v''_r is the atom's velocity in the radial direction after emitting the photon, ν' the frequency of the emitted photon, and α is the angle away from the radial direction. Assuming that our atom can only absorb photons of some specific frequency ν_0 , $h\nu \ll mc$, and $v < c$, the total change in momentum along the radial direction as

$$\Delta mv_r = \frac{h\nu_0}{c} (1 - \cos \alpha). \quad (1.3)$$

Integrating the previous equation over a sphere tells shows that assuming isotropic scattering, the average change in momentum will be $h\nu_0/c$. The same amount for the case of pure absorption. For a given frequency, we can define the opacity accounting for stimulated emission,

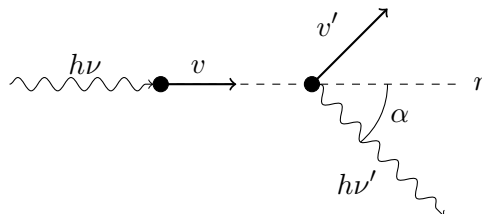
$$\kappa_\nu = \frac{\pi e^2}{m_e c} g f \frac{N_L/g_L - N_U/g_U}{\rho} \phi(\Delta\nu) \quad (1.4)$$

where κ_ν is the opacity with cgs units $\text{cm}^2 \text{g}^{-1}$, m_e is the electrons mass, e the electron charge, $g f$ the oscillator strength, N_L and N_U the lower and upper level populations with corresponding statistical weights g_L and g_U , and $\phi(\Delta\nu)$ is the profile function where

$$\Delta\nu = \nu - \nu_0$$

centered around $\Delta\nu = 0$ and is normalized.

Figure 1.1. Simplified depiction of the momentum transfer by the absorption and emission of a photon.



1.2 SOBOLEV APPROXIMATION

To simplify our calculations, we introduce the Sobolev approximation, one of the most effective means of modeling spectra of astrophysical objects (V.P.Grinin, 2001). The approximation is as follows: for an astrophysical object with large velocity gradients, the interaction between the matter and radiation can be characterized by its local properties. The characteristic length, often called the Sobolev length, is given by

$$s_l = \frac{v_{\text{th}}}{|dv/dl|} \quad (1.5)$$

where dv/dl is the velocity gradient for some direction in the flow and any turbulent velocity is much less than the thermal velocity, otherwise v_{th} would need to be replaced by $\sqrt{v_{\text{th}}^2 + v_{\text{turb}}^2}$, where v_{turb} is the turbulent velocity. For the spherically symmetric winds, dv/dl simplifies to dv/dr (Grinin 2001).

1.3 THE FORCE MULTIPLIER

One of the most useful applications of the Sobolev's approximation was in Caster, Abbott, & Klein (1975, CAK hereafter). They introduce an expression for the radiation force due to a single atomic transition

$$f_{\text{rad,L}} = \frac{\kappa_L F_\nu \Delta\nu}{c} \min(1, 1/\tau_L) \quad (1.6)$$

Where κ_L is the line's opacity, τ_L the line's optical depth, $\Delta\nu = \nu_0 v_{\text{th}}/c$ is the line's Doppler width, and F_ν is the specific flux. The line optical depth for a static atmosphere is given by

$$\tau_L = \int_r^\infty \kappa_L dr, \quad (1.7)$$

and for the expanding case

$$\tau_L = \frac{\kappa_L \rho v_{\text{th}}}{|dv/dr|}. \quad (1.8)$$

CAK introduced a scaling factor for an expanding stellar atmosphere using Sobolev's approximation,

$$t = \frac{\sigma_e \rho v_{\text{th}}}{|dv/dr|}. \quad (1.9)$$

where σ_e is the electron scattering opacity. Note that $t = \tau_L/\kappa_L$. The total force due to lines is

$$f_{\text{rad}} = \frac{\sigma_e}{c} F M(t) \quad (1.10)$$

Where F is the total flux, $M(t)$ is the total force multiplier, defined as

$$M(t) = \sum_{\text{lines}} \frac{F_c \Delta\nu_D}{F} \min\left(\frac{1}{\beta}, \frac{1}{t}\right) \quad (1.11)$$

in CAK, but we often see the total force multiplier as

$$M(t) = \sum_{\text{lines}} \frac{F_c \Delta\nu_D}{F} \frac{1}{t} (1 - e^{-\eta t}) \quad (1.12)$$

(Abbott 1980, Stevens & Kallman 1990; SK90 hereafter), where

$$\eta = \frac{1}{\beta} = \frac{\pi e^2}{m_e c} g f \frac{N_L/g_L - N_U/g_U}{\sigma_e \rho \Delta\nu_D}. \quad (1.13)$$

The summations in equations 1.11 and 1.12 refers to summation over all atomic lines. CAK parameterized these results as

$$M(t) = kt^{-\alpha} \quad (1.14)$$

where k and α are fitted values that are dependent on the stellar atmosphere. The value k is related to the availability of ions to absorb radiation and α is related to the underlying distribution of oscillator strengths. For a star with temperature 40,000 K, $k = 0.0026$ and $\alpha = 0.737$. More generally,

$$k = \frac{v_{\text{th}} N_0 \Gamma(\alpha)}{c (1 - \alpha)} \quad (1.15)$$

where $\Gamma(\alpha)$ is the complete gamma function and N_0 is the normalization factor. CAK and later Owocki, Caster, and Rybicki (1998) would give us an expression for the distribution of the line strengths

$$dN = -N_0 \eta^{\alpha-2} \exp(-\eta/\eta_{\text{max}}) d\eta \frac{d\nu}{\nu} \quad (1.16)$$

where η_{max} is the line strength cut-off.

SK90 demonstrates a case where the ionization structure of the wind is determined by an external source. They had a massive X-ray binary (MXRB) system where the primary object is a massive OB star with a secondary companion that emits X-rays (a neutron star or black hole) via accretion of the wind from the primary star. They show that the amount of ionizing flux from the secondary object has an impact on the force multiplier. We use photoionization parameter to characterize the X-ray radiation

$$\xi = \frac{L_x}{nr^2}, \quad (1.17)$$

where L_x is the source luminosity integrated from 0.1 to 1000 Ry, n the nucleon number density, and r is the distance from the source. Since the ionization structure was assumed to be dominated the X-ray flux from the secondary object, they found that $M(t)$ is a function of ξ as well, reducing the force multiplier at large ξ and thus lowering the resulting wind's velocity. SK90 parameterized k and η_{max} using ξ as

$$k = 0.03 + 0.385 \exp(-1.4\xi^{0.6}) \quad (1.18)$$

and

$$\log_{10} \eta_{\text{max}} \begin{cases} 6.9 \exp(0.16\xi^{0.4}), \log_{10} \xi \leq 0.5, \\ 9.1 \exp(-7.96 \times 10^{-3}\xi), \log_{10} \xi > 0.5, \end{cases} \quad (1.19)$$

This is an interesting result since it shows that moderately ionizing the gas

An alternative parameterization is given to us by Gayley (1995) by considering the ratio of the forces on the bound electrons F_{bound} and free electrons F_{free}

$$\frac{F_{\text{bound}}}{F_{\text{free}}} = \frac{\int_0^{\infty} \sigma_e g f \langle \mu I_{\nu}(\mu) \rangle \phi(\nu) d\nu}{\int_0^{\infty} \sigma_T \langle \mu I_{\nu}(\mu) \rangle d\nu} \quad (1.20)$$

where $\sigma_e = \pi e^2/mc$, $\sigma_T = (8/3)\sigma_e$ is Thompson cross section, and $I_{\nu}(\mu)$ is the incident continuum along direction cosine μ . Skipping many details to not overburden ourselves with notation, Gayley's main result is examining the effects of changing the assumed distribution of line opacities.

Puls et al. (2000) would find that Gayley's formulation to be mostly consistent with CAK's but had would yield incorrect results if not carefully applied. They too found that the underlying distribution of oscillator strengths to be important to the overall impact of the derived force multiplier.

These works have shown that the line force multiplier can be very large using both an analytic and semi-analytic approaches. Where there is a significant amount of UV flux, the force multiplier can be on the order of a few thousand, but we also see that if there is a significant source of X-ray flux, the gas can become over ionized, reducing the effectiveness of line driving (e.g. Proga 2007, and references therein).

CHAPTER 2: METHODS

2.1 ATOMIC DATA

To create a full and rich line list, we merged the atomic data used by XSTAR and the line list curated by Robert L. Kurucz, earlier versions of which were used by Abbott (1980 & 1982) and SK90. We took care when merging these line lists to ensure that no lines were double counted. Figure 2.1 demonstrates the distribution of these lines according to their energies.

2.2 IONIZATION STRUCTURE

We need to calculate the abundances of various ions as a function of ξ for our selected spectral energy distributions (SEDs). In earlier works, the ionization structure was assumed to follow simple analytic formula, such as those found in Mihalas (1978). SK90 would use a full photoionization code to determine the ionization structure of the gas, which would have been the predecessor of the photoionizations code XSTAR. XSTAR is a command-driven computer program for calculating the physical conditions and emission spectra of photoionized gases (Bautista & Kallman 2001).

Using two active galactic nuclei (AGN) SEDs, labeled AGN1 and AGN2 SEDs corresponding to a Type 1 and Type 2 AGN respectively from two different epochs of NGC 5548 (Mehdipour et al. 2015), and two X-ray binary SEDs (Trigo et al. 2013), one in a soft state labeled c6, and the other in a hard state labeled c7, we used XSTAR to generate a grid of models along the thermal equilibrium curve for $\xi = 10^{-2} - 10^5$, similarly to the work of Dyda et al. (2017). These are shown in Figures 2.3, 2.4, 2.5, and 2.6. All abundances assumed to be solar abundances.

2.3 CALCULATING THE FORCE MULTIPLIER

Combining our newly constructed atomic dataset and our ion abundances determined from XSTAR, we take this data and apply them to equations 1.13 and 1.12, the only additional assumption, similar to SK90, to make is the level occupancy, which we assume follows the Boltzmann excitation equation

$$\frac{N_L}{N_U} = \frac{g_L}{g_U} e^{-(E_U - E_L)/kT}. \quad (2.1)$$

Figure 2.1. Shown here is the distribution of the entries in our atomic datasets. Kurucz's shown in red, XSTAR's shown in blue, and the total list after they were carefully merged shown in black.

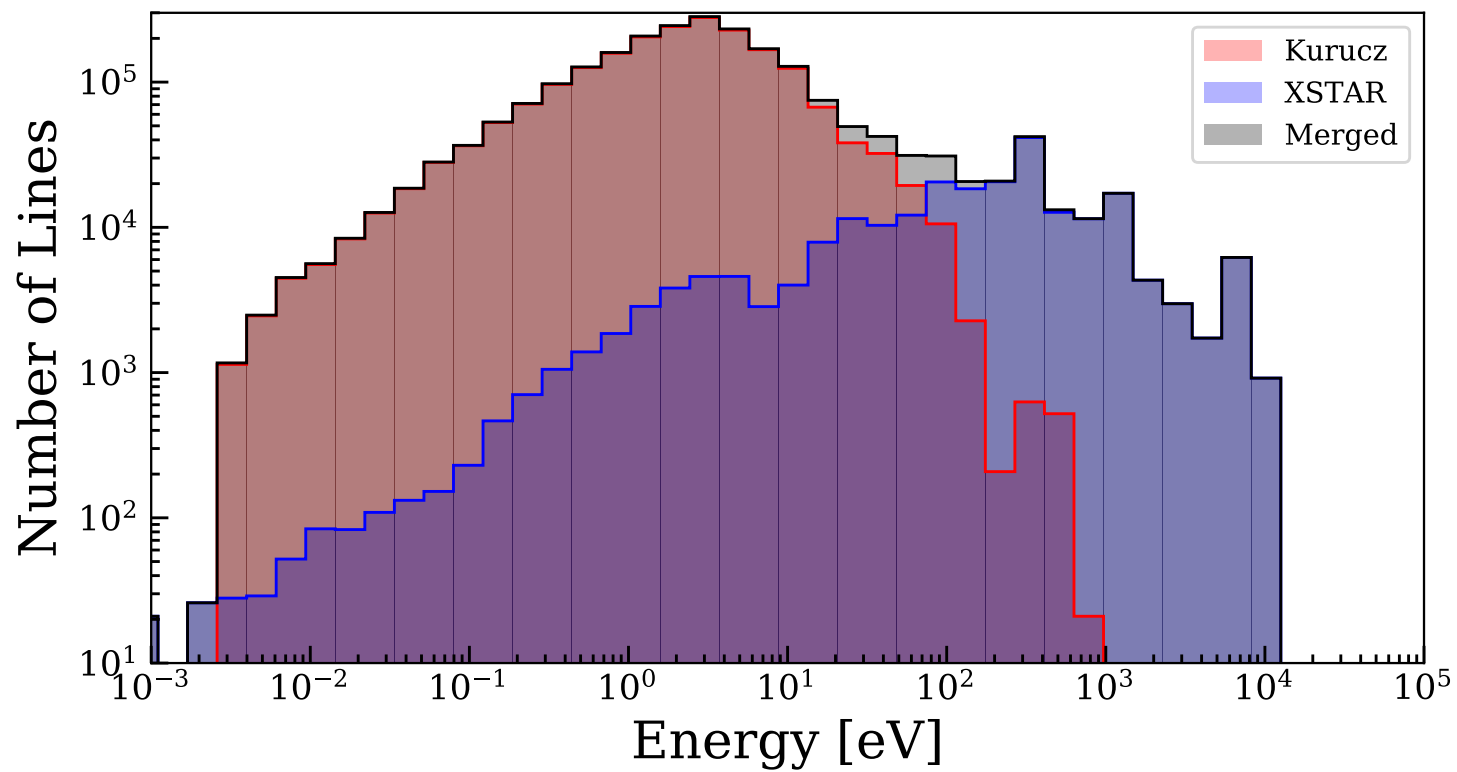


Figure 2.2. The top panels show the SEDs AGN1, AGN2 (left), c6, and c7 (right) with the flux in arbitrary units. The bottom panels shows what fraction of the total energy is in each energy band (IR, optical, UV, X-ray, and range integrated for our definition of ξ in red, green, purple, dark blue-grey, and orange respectively).

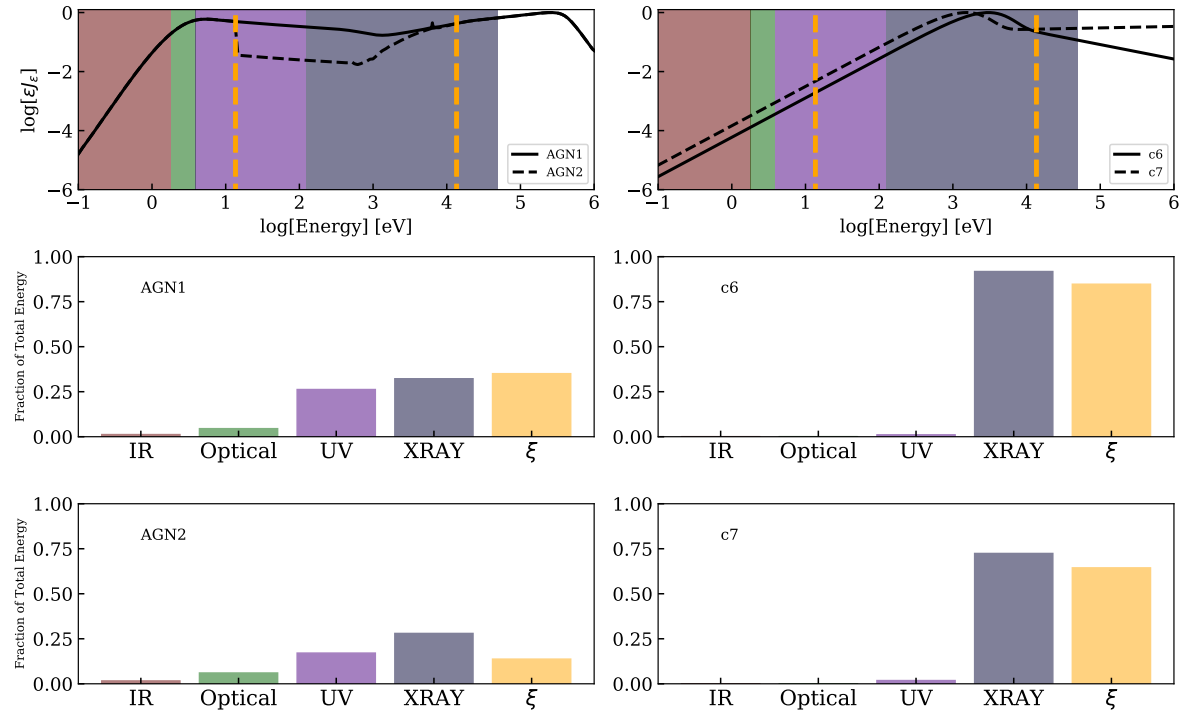


Figure 2.3. Shown here is relative ion abundances for determined by XSTAR for AGN1.

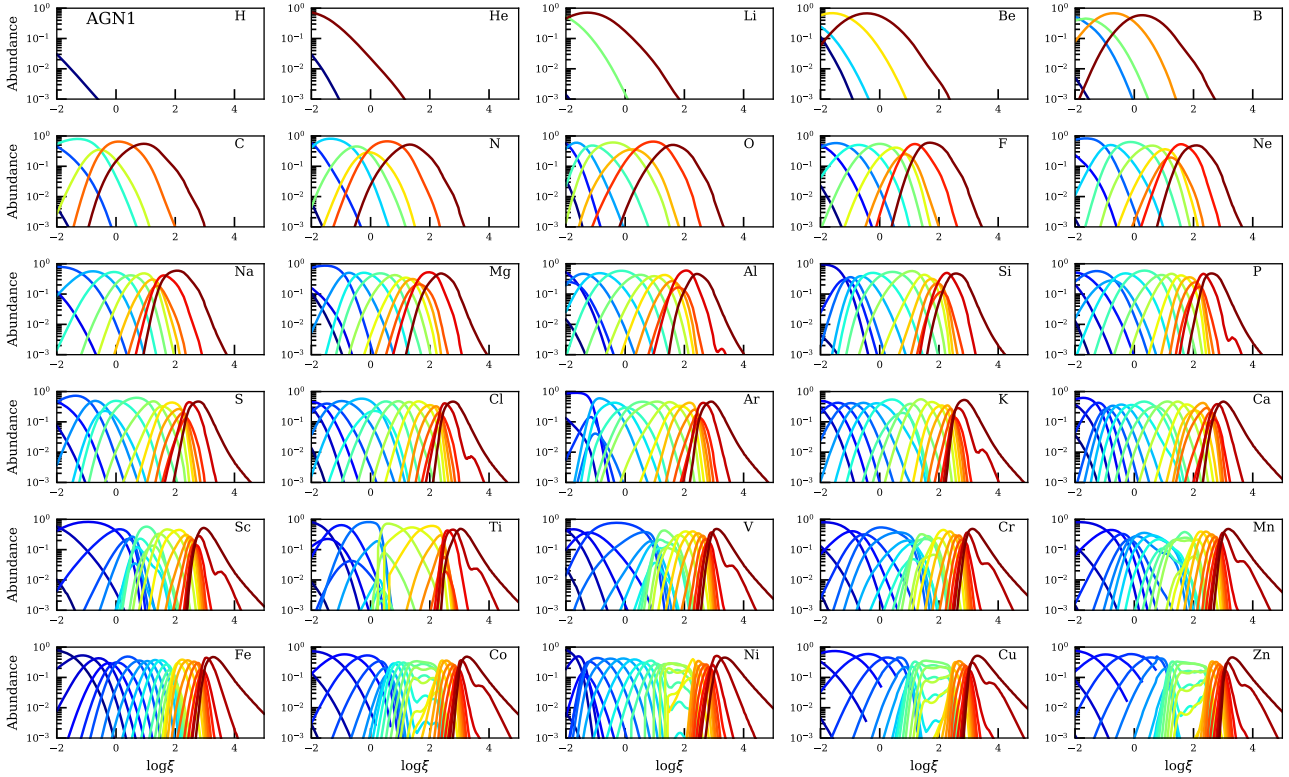


Figure 2.4. Same as Figure 2.3 but for AGN2.

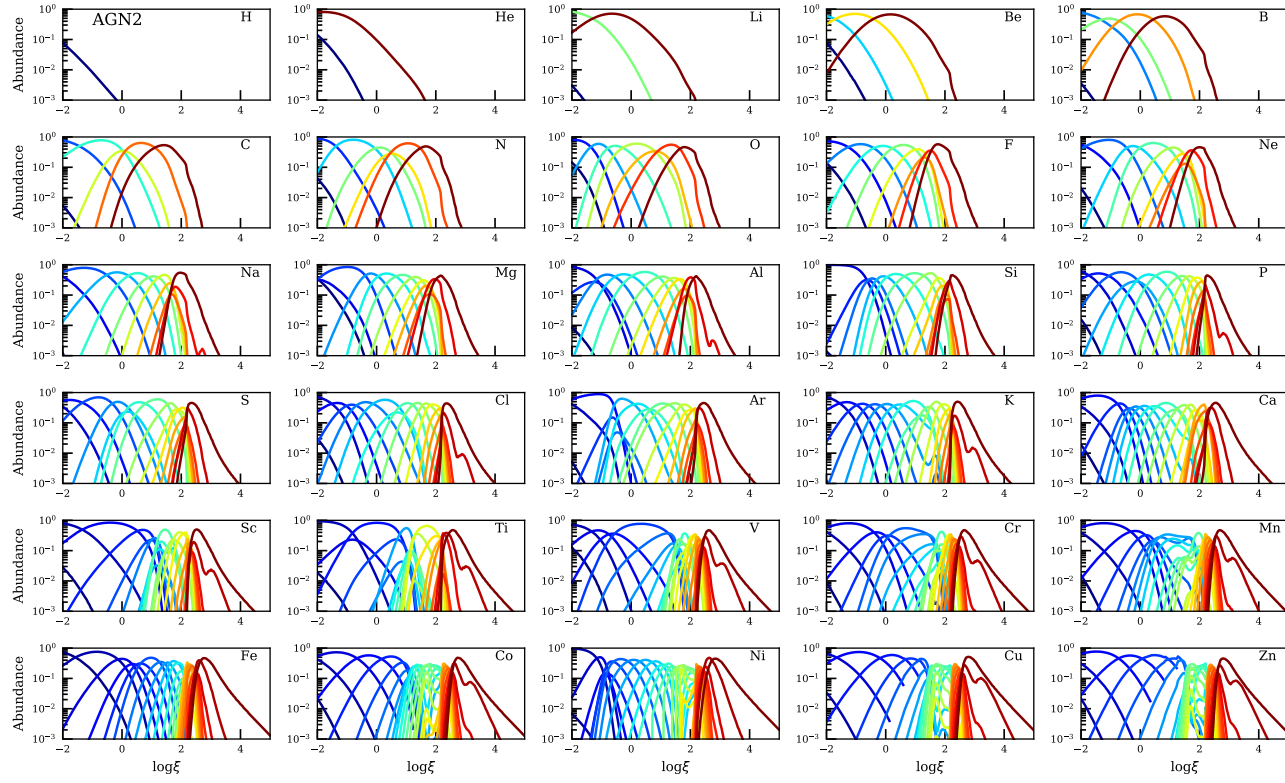


Figure 2.5. Same as Figure 2.3 but for c6.

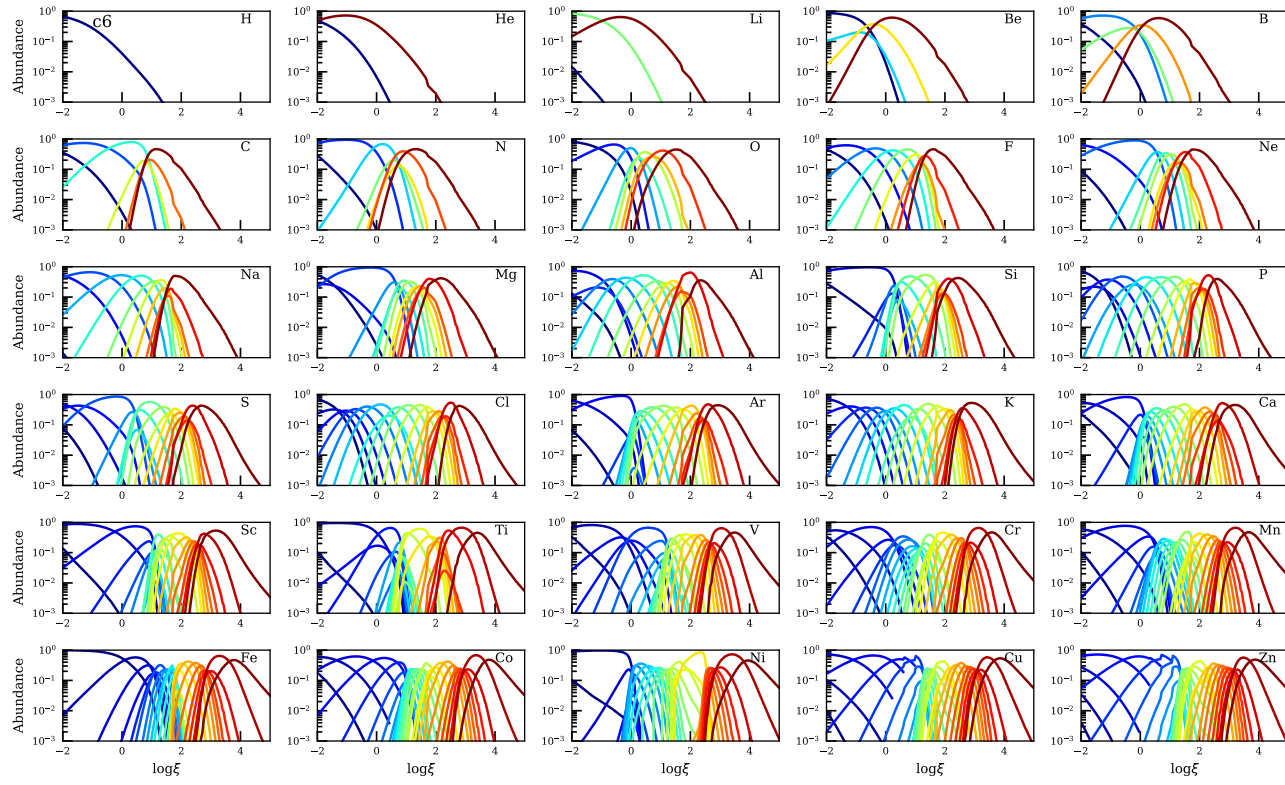
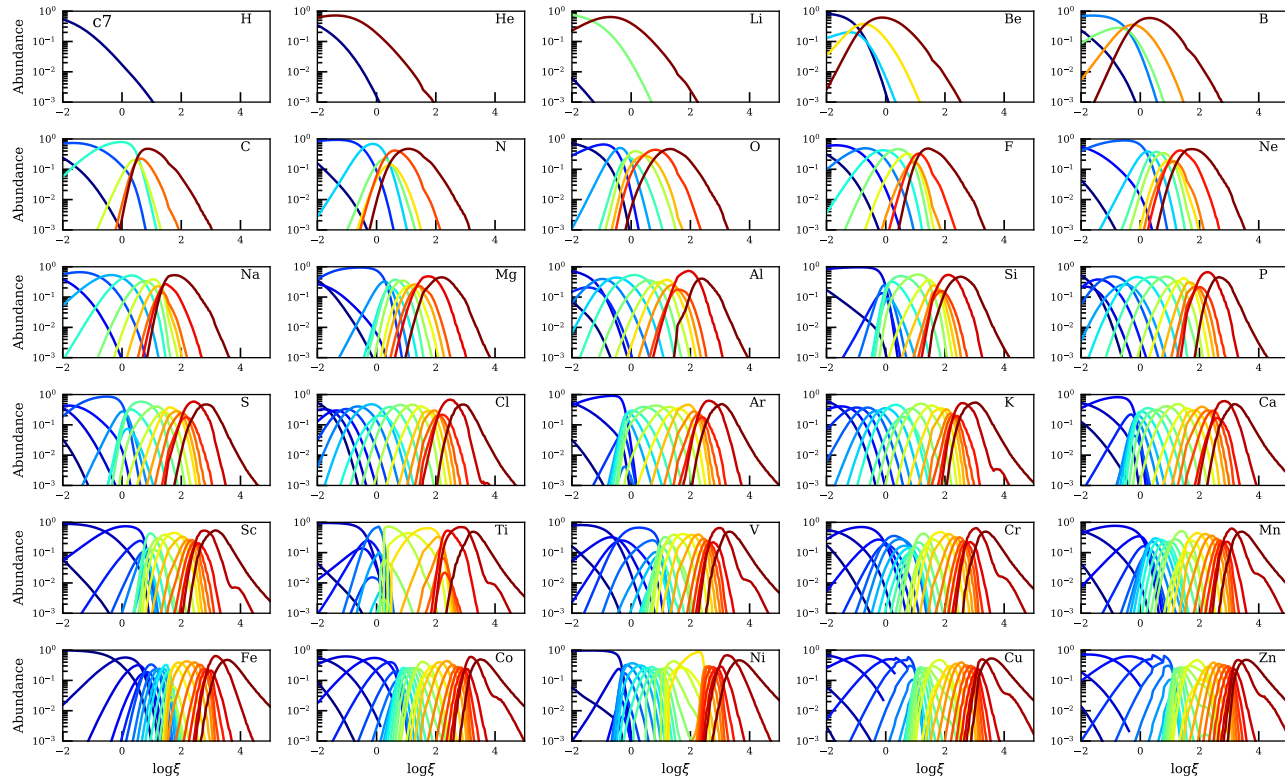


Figure 2.6. Same as Figure 2.3 but for c7.



CHAPTER 3: RESULTS

We present our main conclusions about the total force multiplier for our AGN and XRB type SEDs in Figures 3.1 and 3.2. In Figures 3.5-3.12 we present how much each element and their ion contributes to the total force multiplier. Tables 3.1-3.4 present the top five contributors to the total force multiplier. and 3.2.

Figure 3.1. Shown is the force multiplier $M(t, \xi)$ for our four SEDs, labeled in the top right of each panel. The x-axis is our optical depth parameter t , and the lines indicate differences $\Delta \log \xi = 1$, stepping from -2 to 5, dashed for negative value, solid for positive. The color is to give some indication relative value, going from low (blue) to high (red).

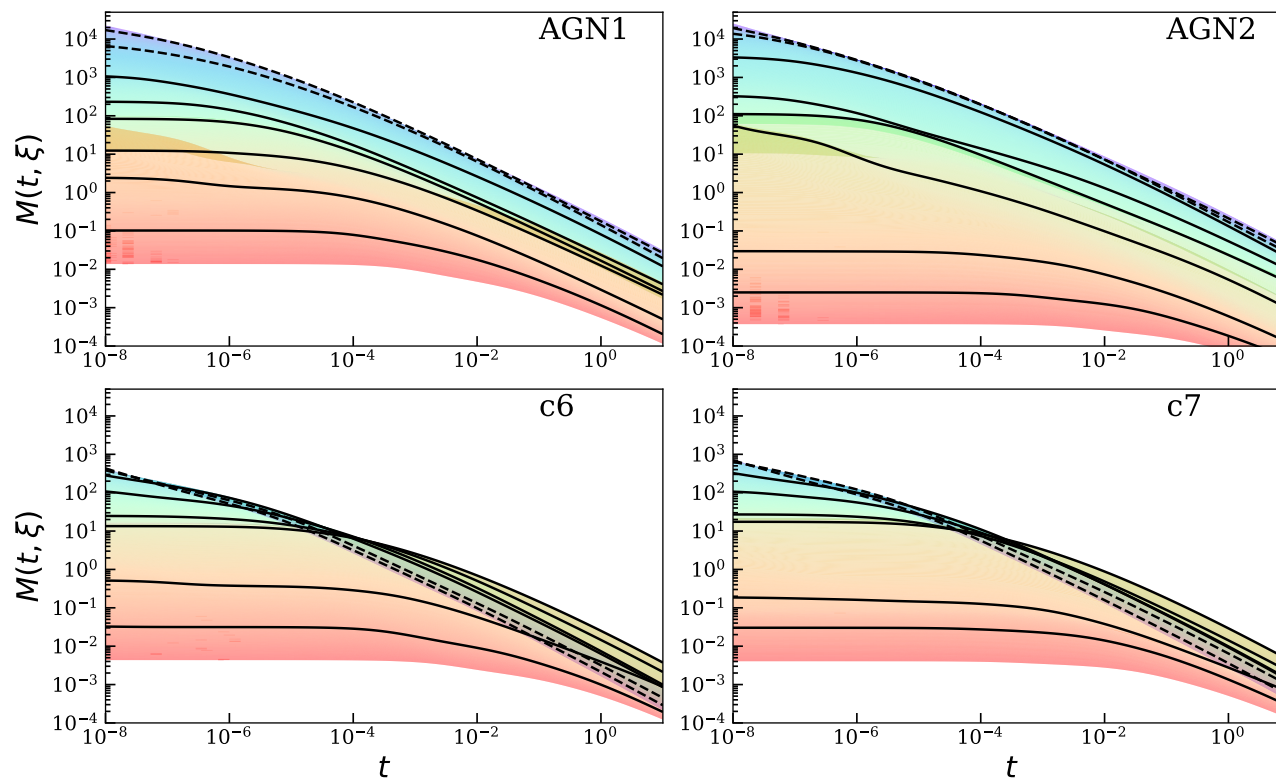


Figure 3.2. Shown is the force multiplier $M(t, \xi)$ for our four SEDs, labeled in the top right of each panel. The x-axis is our photoionization parameter ξ , and the lines indicate differences $\Delta \log t = 1$, stepping from -8 to 2, dashed for negative values, solid for positive. The color is to give some indication relative value, going from low (blue) to high (red).

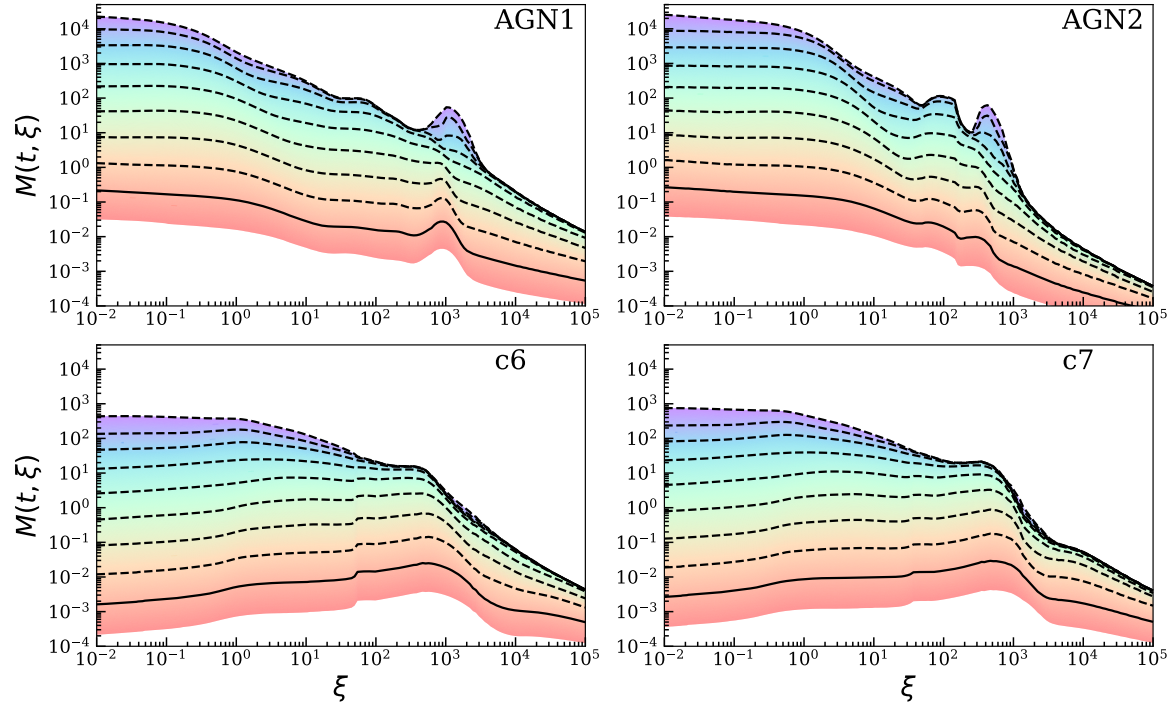


Figure 3.3. The left panels correspond to AGN1 and the right panels correspond to AGN2. The solid black line is the thermal equilibrium curve determined by XSTAR corresponding to the right y-axis. The solid blue, dashed red, and dash-dotted green line correspond to the total force multiplier, UV component of the force multiplier, and X-ray component of the force multiplier respectively. The shaded region in the top two figures indicates where we'd expect the gas to become thermally unstable using the condition $\partial \ln T / \partial \ln \xi > 1$ (Field 1965). The bottom show η_{\max} for all lines, UV lines, and X-ray lines in solid blue, dashed red, and dash-dotted green respectively.

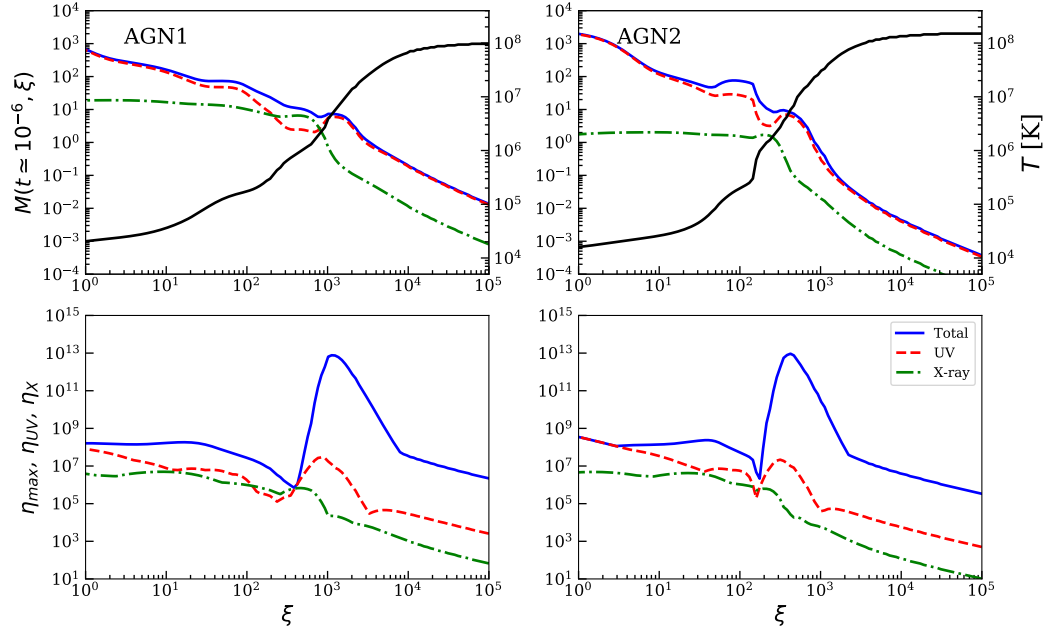


Figure 3.4. The left panels correspond to c6 and the right panels correspond to c7. The solid black line is the thermal equilibrium curve determined by XSTAR corresponding to the right y-axis. The solid blue, dashed red, and dash-dotted green line correspond to the total force multiplier, UV component of the force multiplier, and X-ray component of the force multiplier respectively. The shaded region in the top two figures indicates where we'd expect the gas to become thermally unstable using the condition $\partial \ln T / \partial \ln \xi > 1$ (Field 1965). The bottom show η_{\max} for all lines, UV lines, and X-ray lines in solid blue, dashed red, and dash-dotted green respectively.

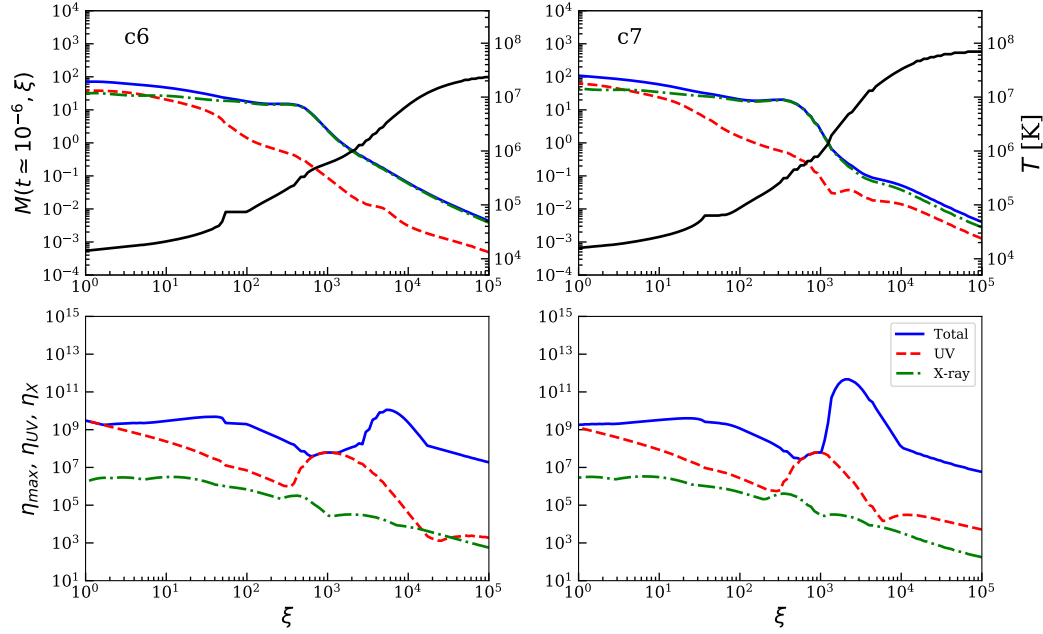


Figure 3.5. We present details about the force multiplier due to individual elements for SED AGN1. We show only elements that contribute at least 10% of the total force multiplier for any value of ξ .

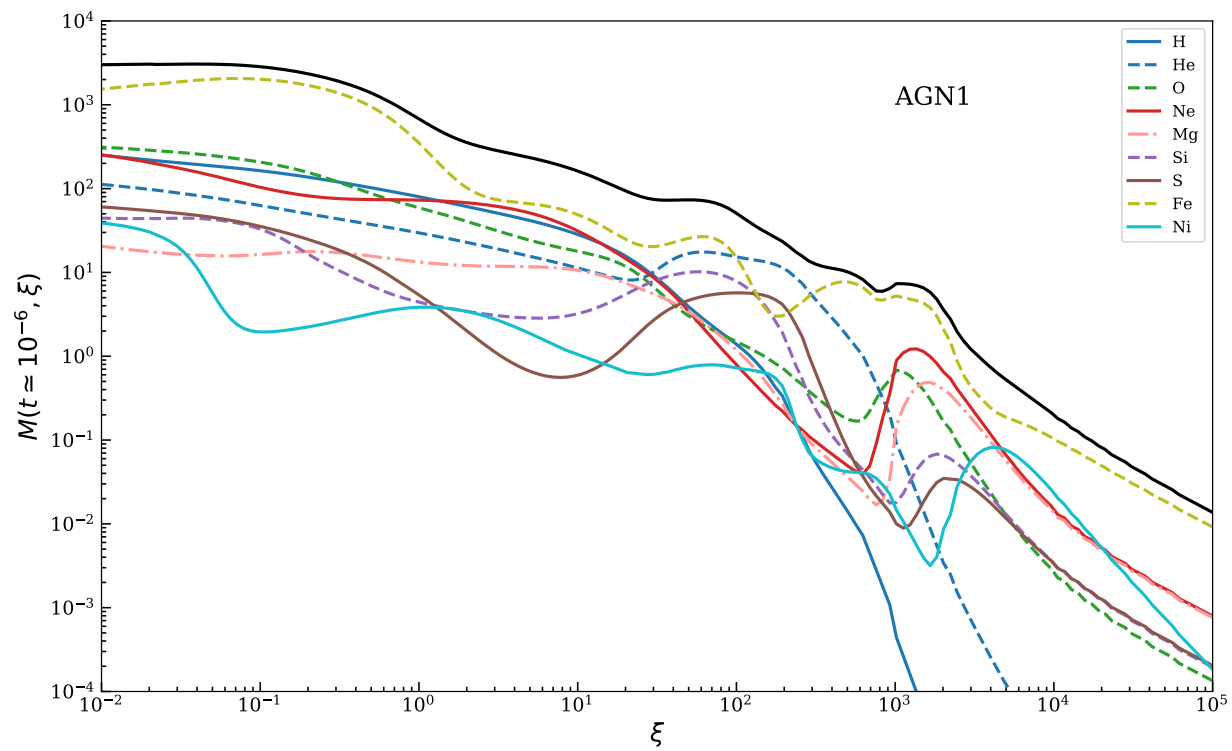


Figure 3.6. We present details about the force multiplier due to individual ions for SED AGN1. We show only ions that contribute at least 10% of the total force multiplier for any value of ξ .

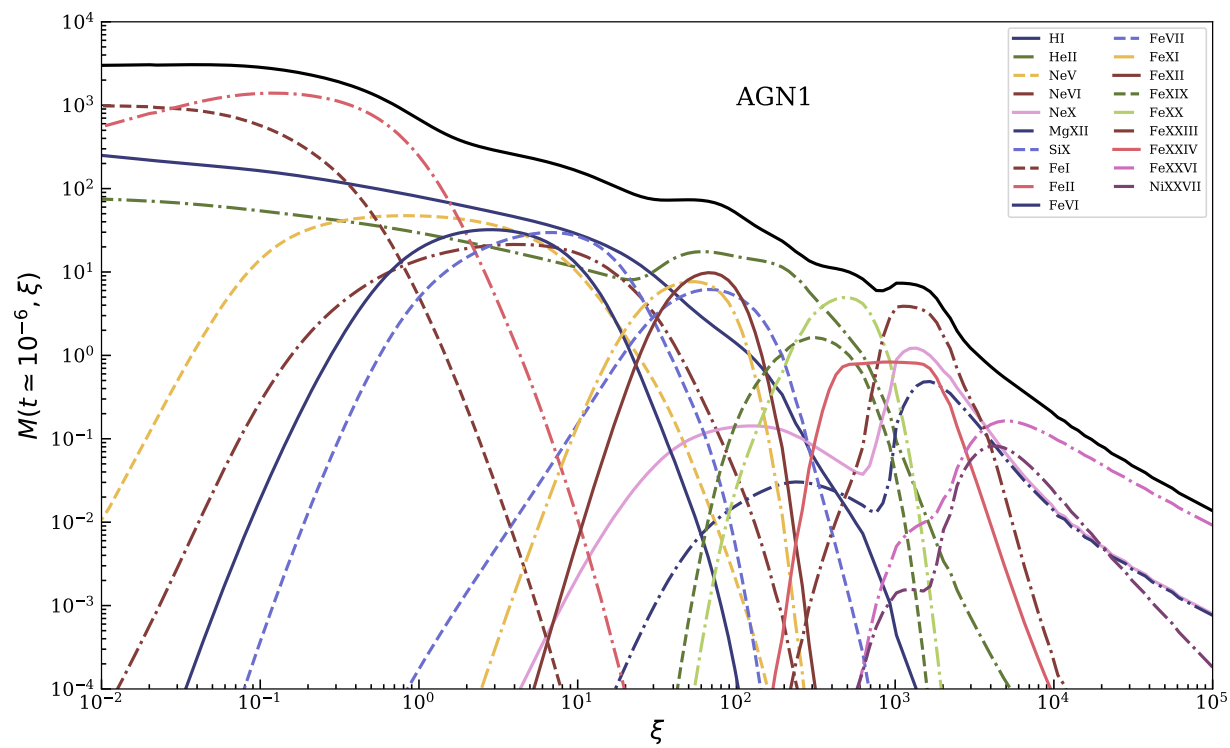


Figure 3.7. Same as Figure 3.5 but for AGN2.

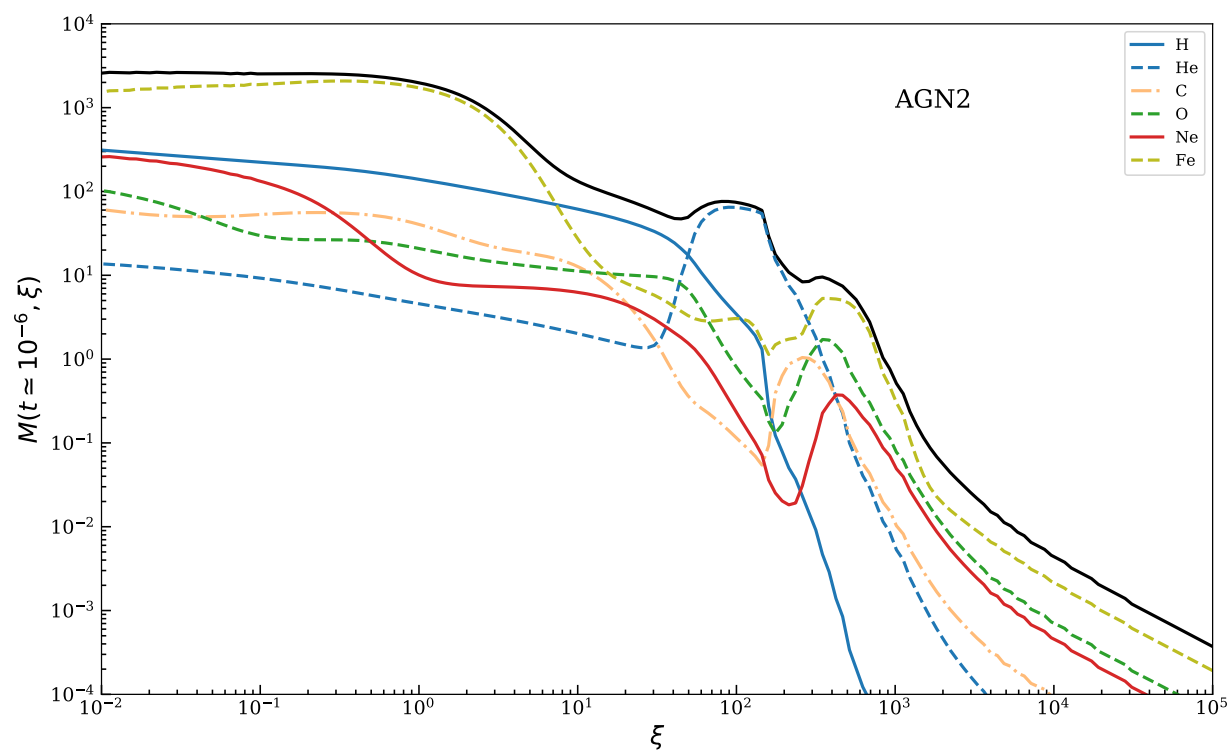


Figure 3.8. Same as Figure 3.6 but for AGN2.

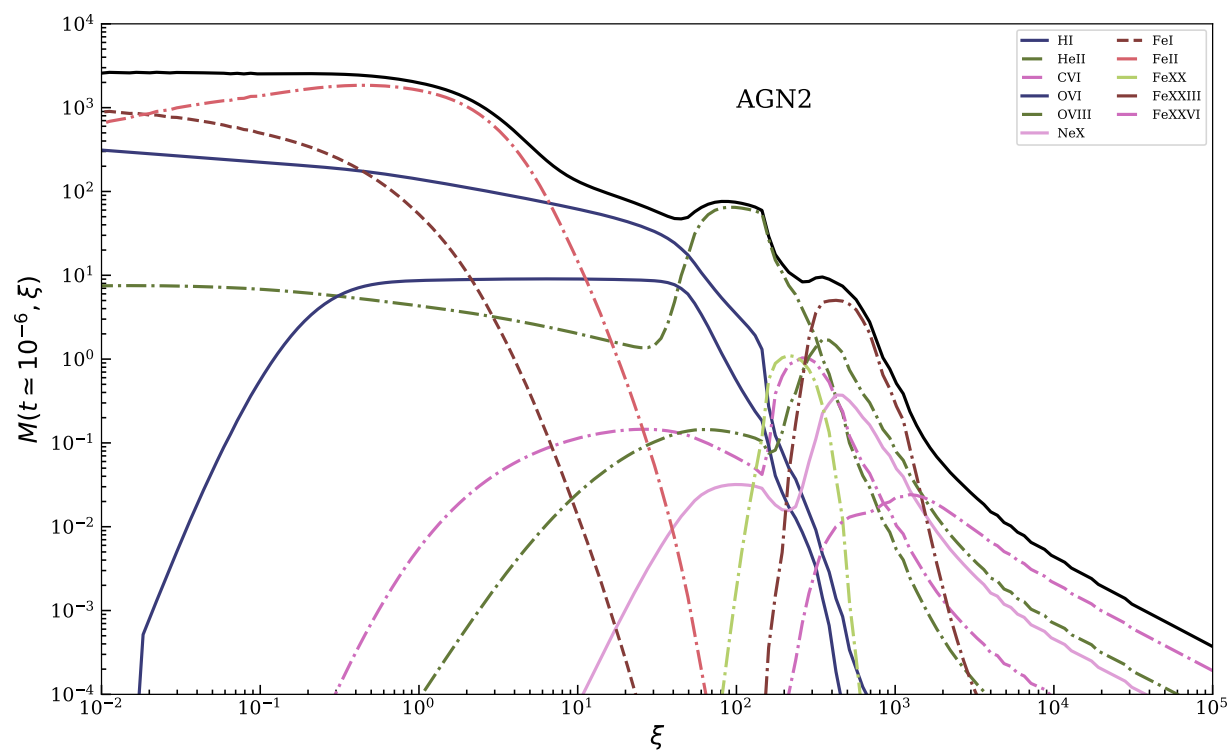


Figure 3.9. Same as Figure 3.5 but for c6.

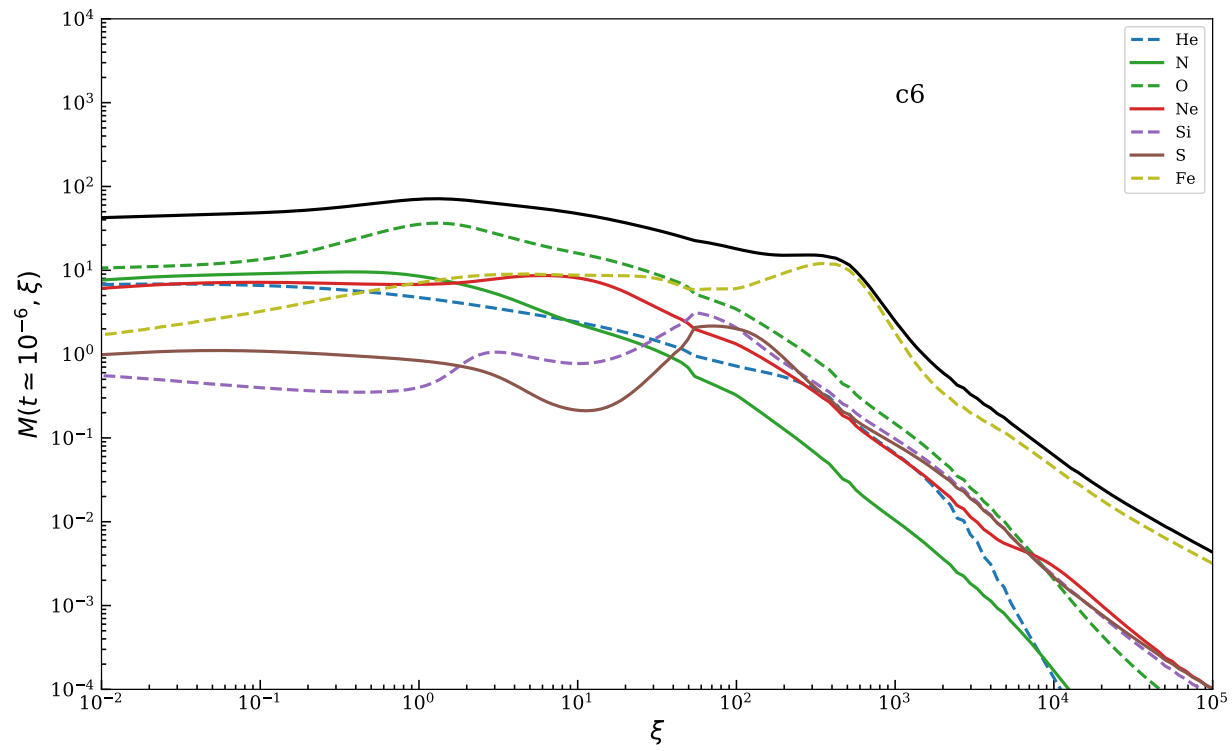


Figure 3.10. Same as Figure 3.6 but for c6.

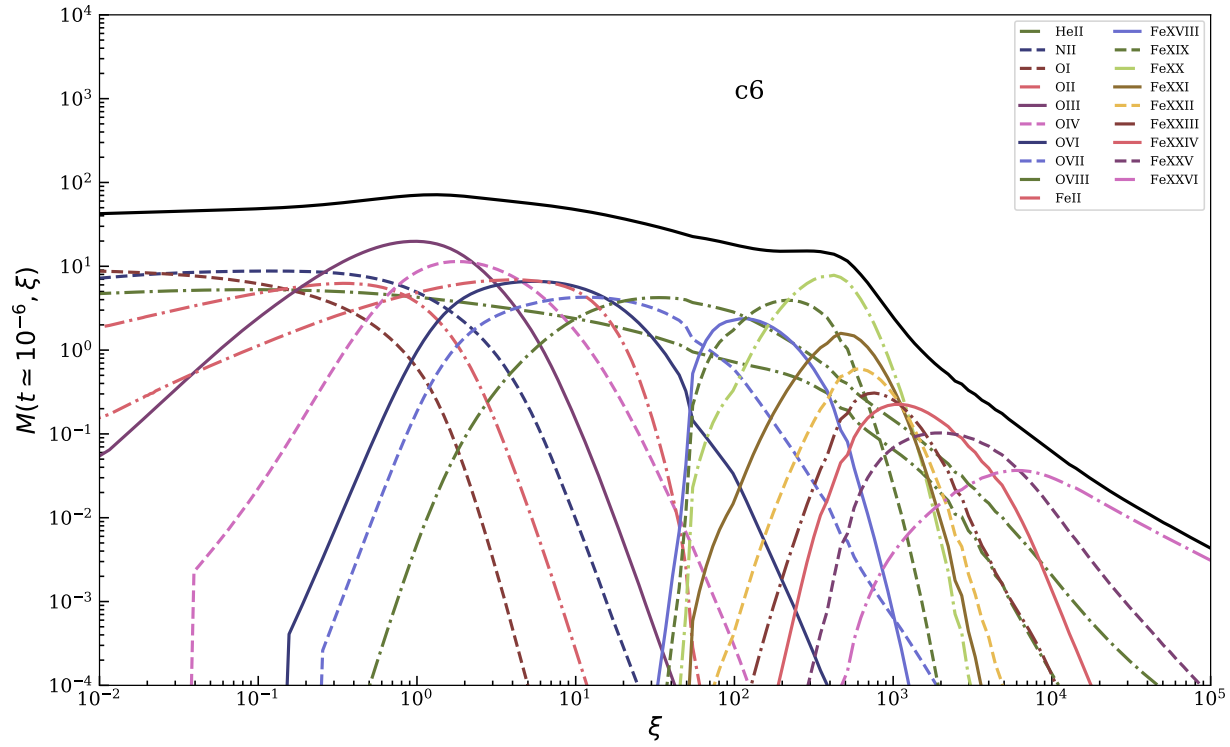


Figure 3.11. Same as Figure 3.5 but for $c7$.

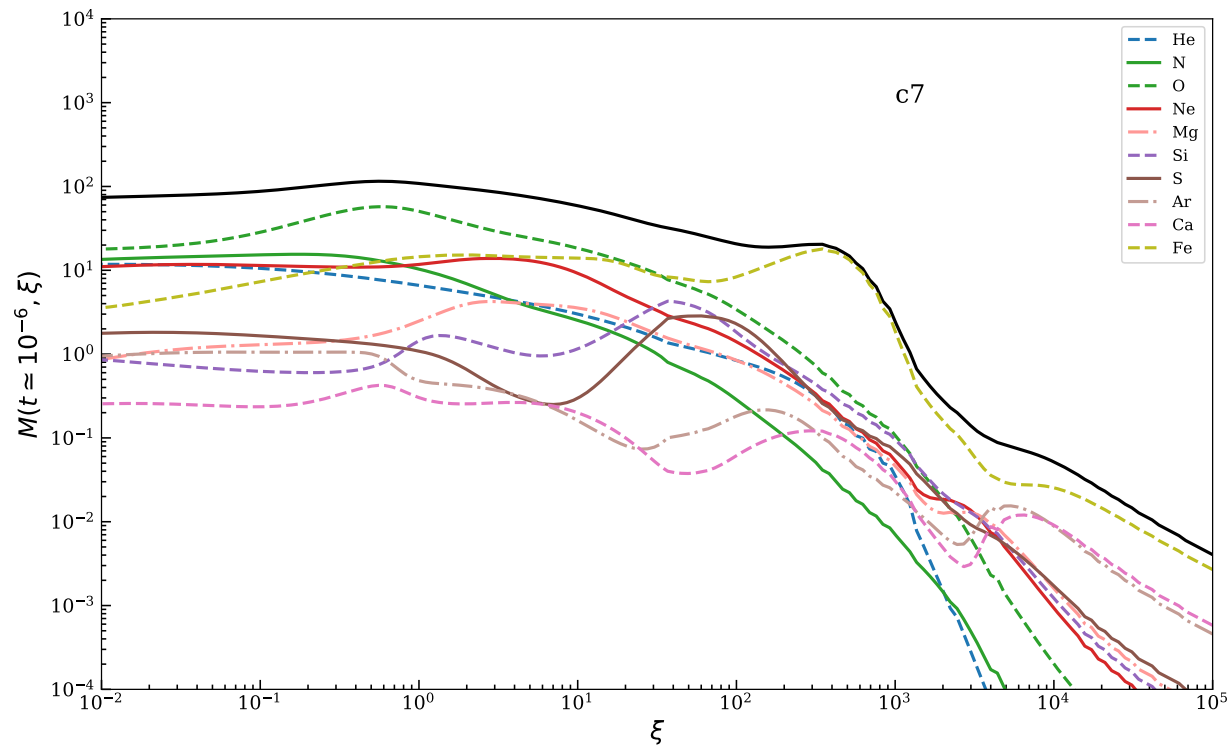


Figure 3.12. Same as Figure 3.6 but for c7.

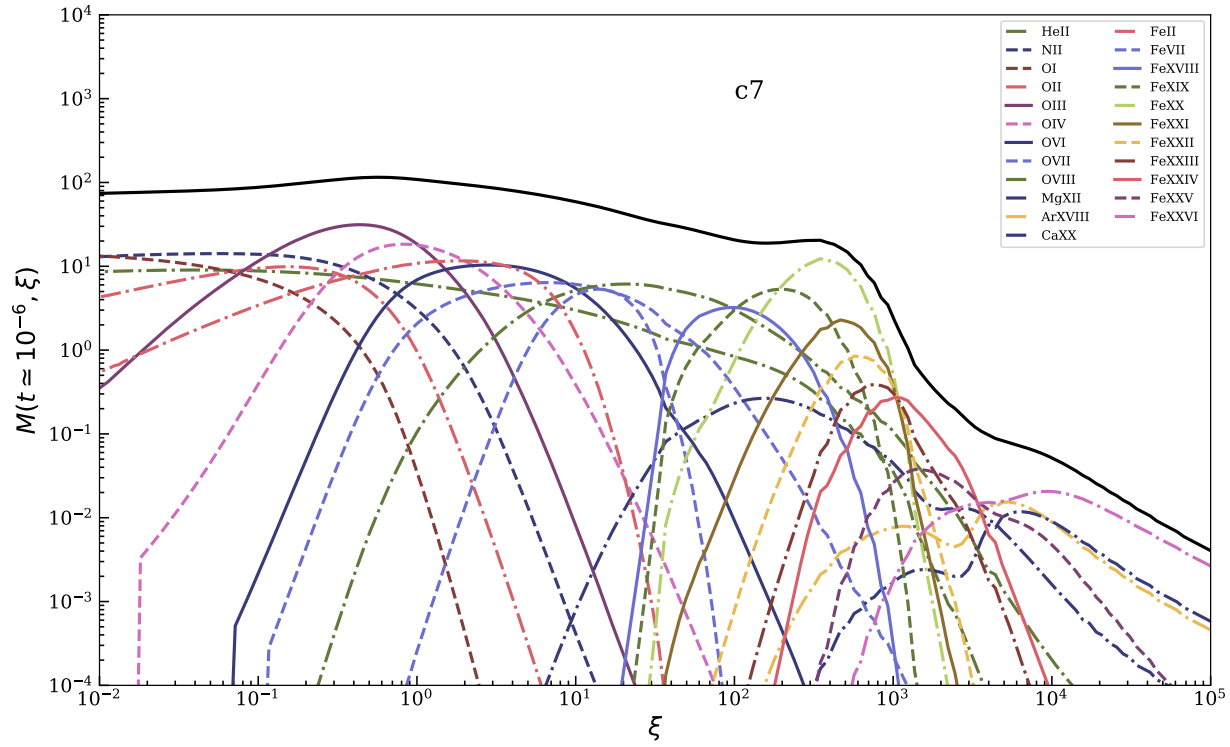


Table 3.1. Table showing the top five contributors to the force multiplier for AGN1 with $t = 10^{-6}$ for various values of ξ . The left column for each block indicates the ion the line belongs, then its wavelength in angstroms, and then the value force multiplier for just that line $M_L(t, \xi)$.

AGN1		
$t = 10^{-6}$	$\log(\xi) \simeq 0$	$M_{total}(t, \xi) = 522$
Ion	Wavelength (\AA)	$M_L(t, \xi)$
HI	1216	5.051
HI	1026	4.768
CIV	1550	1.550
NV	1239	1.355
OVI	1037	1.224 d
$t = 10^{-6}$	$\log(\xi) \simeq 1$	$M_{total}(t, \xi) = 123$
Ion	Wavelength (\AA)	$M_L(t, \xi)$
HI	1216	4.771
NeVI	401	1.02
OVI	150	0.945
OVII	21	0.724
CV	40	0.6812
$t = 10^{-6}$	$\log(\xi) \simeq 2$	$M_{total}(t, \xi) = 24$
Ion	Wavelength (\AA)	$M_L(t, \xi)$
OVIII	19	0.604
SiX	303	0.399
FeXI	180	0.340
FeXII	202	0.330
FeXIV	284	0.290
$t = 10^{-6}$	$\log(\xi) \simeq 3$	$M_{total}(t, \xi) = 20$
Ion	Wavelength (\AA)	$M_L(t, \xi)$
FeXXIII	777	7.328
FeXXII	1157	3.546
FeXXII	1344	2.640
FeXXII	3738	2.172
FeXXII	9586	1.561

Table 3.2. Same as Table 3.1 but for AGN2.

AGN2		
$t = 10^{-6}$	$\log(\xi) \simeq 0$	$M_{total}(t, \xi) = 1635$
Ion	Wavelength (\AA)	$M_L(t, \xi)$
HI	1216	5.992
HI	1026	5.769
CIV	1550	1.840
CIII	977	1.562
NV	1239	1.520
$t = 10^{-6}$	$\log(\xi) \simeq 1$	$M_{total}(t, \xi) = 117$
Ion	Wavelength (\AA)	$M_L(t, \xi)$
HI	1216	7.522
HI	1026	4.023
CIV	1548	2.227
NV	1239	1.907
OVI	1038	1.849
$t = 10^{-6}$	$\log(\xi) \simeq 2$	$M_{total}(t, \xi) = 9.2$
Ion	Wavelength (\AA)	$M_L(t, \xi)$
HI	6563	0.409
OVI	1032	0.171
FeXI	180	0.096
FeX	174	0.089
FeXII	187	0.089
$t = 10^{-6}$	$\log(\xi) \simeq 2.6$	$M_{total}(t, \xi) = 22$
Ion	Wavelength (\AA)	$M_L(t, \xi)$
FeXXIII	1157	6.200
FeXXIII	1345	4.725
FeXXIII	3739	3.909
FeXXIII	9587	2.193
OVIII	1303	0.416

Table 3.3. Same as Table 3.1 but for c6.

c6		
$t = 10^{-6}$	$\log(\xi) \simeq 0$	$M_{total}(t, \xi) = 78$
Ion	Wavelength (Å)	$M_L(t, \xi)$
OIV	22.74	1.916
OIII	23.07	1.674
OIII	23.10	1.634
OIV	22.77	1.501
OV	22.37	1.495
$t = 10^{-6}$	$\log(\xi) \simeq 1$	$M_{total}(t, \xi) = 48$
Ion	Wavelength (Å)	$M_L(t, \xi)$
OVII	21.60	2.181
OVI	22.02	4.023
OVI	22.04	2.227
OVIII	18.97	1.907
OV	22.37	1.849
$t = 10^{-6}$	$\log(\xi) \simeq 2$	$M_{total}(t, \xi) = 17$
Ion	Wavelength (Å)	$M_L(t, \xi)$
OVIII	18.967	1.160
OVIII	18.973	0.662
NeX	12.13	0.391
FeXVII	15.02	0.363
FeXVIII	14.21	0.326
$t = 10^{-6}$	$\log(\xi) \simeq 2.5$	$M_{total}(t, \xi) = 15$
Ion	Wavelength (Å)	$M_L(t, \xi)$
FeXX	12.89	0.579
FeXX	12.83	0.445
FeXX	12.98	0.372
OVIII	18.97	0.358
FeXXI	12.28	0.329

Table 3.4. Same as Table 3.1 but for c7.

c7		
$t = 10^{-6}$	$\log(\xi) \simeq 0$	$M_{total}(t, \xi) = 113$
Ion	Wavelength (Å)	$M_L(t, \xi)$
OV	22.37	3.131
OIV	22.74	2.942
OIV	22.77	2.353
OVI	22.02	2.111
OVI	22.03	2.018
$t = 10^{-6}$	$\log(\xi) \simeq 1$	$M_{total}(t, \xi) = 59$
Ion	Wavelength (Å)	$M_L(t, \xi)$
OVII	21.60	3.194
OVIII	18.97	2.496
OVII	18.63	1.571
OVIII	18.97	1.567
CVI	33.73	1.287
$t = 10^{-6}$	$\log(\xi) \simeq 2$	$M_{total}(t, \xi) = 20$
Ion	Wavelength (Å)	$M_L(t, \xi)$
OVIII	18.967	1.246
OVIII	18.973	0.684
NeX	12.13	0.455
FeXIX	13.53	0.385
FeXVII	15.02	0.374
$t = 10^{-6}$	$\log(\xi) \simeq 2.5$	$M_{total}(t, \xi) = 21$
Ion	Wavelength (Å)	$M_L(t, \xi)$
FeXX	12.89	0.947
FeXX	12.83	0.737
FeXX	12.98	0.582
FeXXI	12.28	0.483
FeXX	12.86	0.353

CHAPTER 4: CONCLUSION, DISCUSSION, & FUTURE WORK

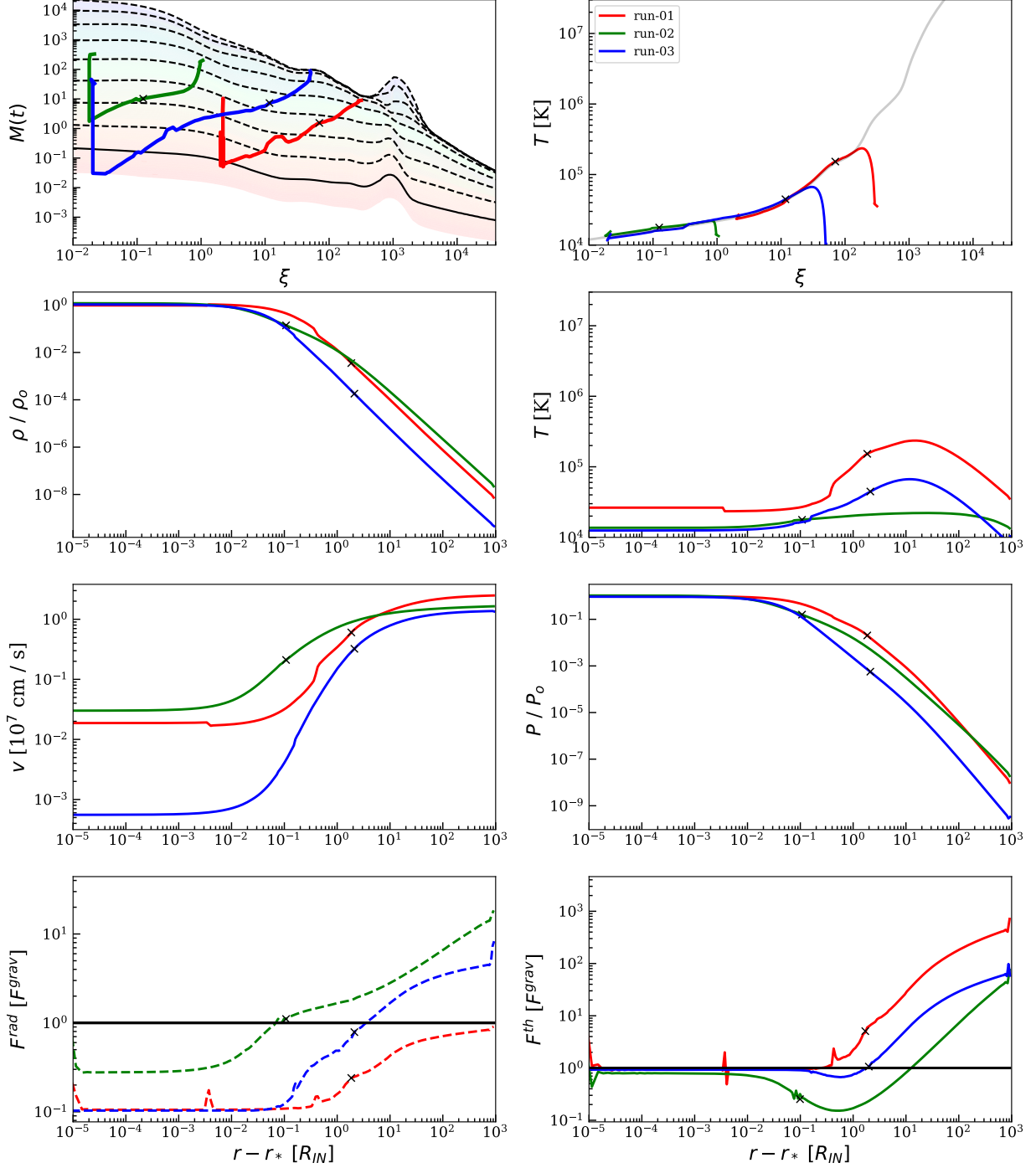
We confirm the claim made by Puls et al. (1999) that the line force is a consequence of the small contributions of many thousands of lines rather than a consequence of only a few.

We see that there is a secondary enhancement in the force multiplier for all SEDs, most prominently for the SED AGN1 and AGN2, in the region $\log \xi \sim 2.5$. This could lead to a secondary region where line driving becomes efficient.

Spectral lines belonging to Fe and O seem to be primary contributors to the force multiplier when the gas is highly ionized ($\xi > 100$), but we see contribution from many different elements when the gas is less ionized ($\xi < 100$). The force multiplier results for the XRB cases show us that X-ray lines can also play an important role in line driving since most of the total flux is in the X-ray band for SED c6 and c7.

Future work will involve taking the findings shown here and implementing them into the magnetohydrodynamic (MHD) code ATHENA++ (Gardiner & Stone 2005, 2008). We wish to characterize the regimes where line driving is important in the description of the dynamics of the resulting wind and similarly to the work of Waters et al. 2017, create synthetic spectra to compare with observation. Preliminary 1D results will be shown in Figure 4.1, but with the goal of 2D and 3D simulations. more information can be found in the Appendix and Dannen & Proga (2018, in prep).

Figure 4.1. Preliminary results from ATHENA++ using both the heating and cooling model described in Dyda et al. (2017) and force multiplier values shown in Chapter 3. Models run-01 and run-02 correspond to wind from a central object with $M = 1M_\odot$ and $M = 10M_\odot$ for run-03. $\rho_0 = 1.30 \times 10^{-13}$ run-01 and run-02, and $\rho_0 = 3.27 \times 10^{-21}$ for run-03. R_{IN} is 4.60×10^{12} cm for run-01, 1.46×10^{12} cm for run-02, and 2.91×10^{20} cm for run-03. More detailed results will be shown in Dannen & Proga (2018, in prep.)



APPENDIX: MHD BASICS

We seek to incorporate our force multiplier results shown in Chapter 3 with our previous work from Dyda et al. (2017). We seek to use the magnetohydrodynamic code ATHENA++ (Gardiner & Stone 2005, 2008), heating and cooling rates determined by the photoionization code XSTAR, and our newly derived force multipliers to determine if it's possible to have a line driven wind. The basic fluid equations that need to be solved

$$\frac{\partial \rho}{\partial t} + \nabla \cdot (\rho \mathbf{v}) = 0, \quad (\text{A.1})$$

$$\frac{\partial \rho \mathbf{v}}{\partial t} + \nabla \cdot (\rho \mathbf{v} \mathbf{v} + \mathbf{P}) = -\rho \nabla \Phi + \rho \mathbf{F}^{\text{rad}}, \quad (\text{A.2})$$

$$\frac{\partial E}{\partial t} + \nabla \cdot ((E + P)\mathbf{v}) = -\rho \mathbf{v} \cdot \nabla \Phi - \rho \mathcal{L} + \rho \mathbf{v} \cdot \mathbf{F}^{\text{rad}} \quad (\text{A.3})$$

where ρ is the fluid density, \mathbf{v} is the fluid velocity, \mathbf{P} is the diagonal tensor with the components of P the gas pressure, $\Psi = -GM/r$ is the gravitational potential due to the central object, and $E = 1/2\rho|\mathbf{v}|^2 + \mathcal{E}$ is the energy where $\mathcal{E} = P/(\gamma - 1)$ is the internal energy, and \mathcal{L} is the cooling rate. We adopt an equation of state $P = \rho^\gamma$ Where the radiation force can be split into the electron scattering and line components. The radiation force due to electron scattering is

$$\mathbf{F}_e^{\text{rad}} = \oint \left(\hat{\mathbf{n}} \frac{\sigma_e I d\Omega}{c} \right), \quad (\text{A.4})$$

and the radiation force due to lines

$$\mathbf{F}_L^{\text{rad}} = \oint \left(M(t, \xi) \hat{\mathbf{n}} \frac{\sigma_e I d\Omega}{c} \right), \quad (\text{A.5})$$

making the total radiation force

$$\mathbf{F}^{\text{rad}} = \oint \left([1 + M(t, \xi)] \hat{\mathbf{n}} \frac{\sigma_e I d\Omega}{c} \right) \quad (\text{A.6})$$

(Dyda & Proga 2018a, 2018b).

BIBLIOGRAPHY

- [1] D. C. Abbott. The theory of radiatively driven stellar winds. I - A physical interpretation. , 242:1183–1207, December 1980.
- [2] D. C. Abbott. The theory of radiatively driven stellar winds. II - The line acceleration. , 259:282–301, August 1982.
- [3] M. A. Bautista and T. R. Kallman. The XSTAR Atomic Database. , 134:139–149, May 2001.
- [4] J. I. Castor, D. C. Abbott, and R. I. Klein. Radiation-driven winds in Of stars. *The Astrophysical Journal*, 195:157, 1975.
- [5] S. Dyda, R. Dannen, T. Waters, and D. Proga. Irradiation of astrophysical objects - SED and flux effects on thermally driven winds. , 467:4161–4173, June 2017.
- [6] G. B. Field. Thermal Instability. , 142:531, August 1965.
- [7] K. G. Gayley. An Improved Line-Strength Parameterization in Hot-Star Winds. , 454:410, November 1995.
- [8] V. P. Grinin. Sobolev’s Approximation. *Astrophysics*, 44:402–410, July 2001.
- [9] H. J. G. L. M. Lamers and J. P. Cassinelli. *Introduction to Stellar Winds*. June 1999.
- [10] M. Mehdipour, J. S. Kaastra, G. A. Kriss, M. Cappi, P.-O. Petrucci, B. De Marco, G. Ponti, K. C. Steenbrugge, E. Behar, S. Bianchi, G. Branduardi-Raymont, E. Costantini, J. Ebrero, L. Di Gesu, G. Matt, S. Paltani, B. M. Peterson, F. Ursini, and M. Whewell. Anatomy of the AGN in NGC 5548. VII. Swift study of obscuration and broadband continuum variability. , 588:A139, April 2016.
- [11] D. Mihalas. *Stellar atmospheres 2nd edition*. 1978.
- [12] D. Proga, J. M. Stone, and J. E. Drew. Radiation-driven winds from luminous accretion discs. , 295:595, April 1998.
- [13] D. Proga, J. M. Stone, and T. R. Kallman. Dynamics of Line-driven Disk Winds in Active Galactic Nuclei. , 543:686–696, November 2000.
- [14] J. Puls, U. Springmann, and M. Lennon. Radiation driven winds of hot luminous stars. XIV. Line statistics and radiative driving. , 141:23–64, January 2000.
- [15] M. D. Trigo, L. Boirin, S. Migliari, J. Miller-Jones, A. Parmar, and L. Sidoli. Variability of winds in X-ray binaries. In C. M. Zhang, T. Belloni, M. Méndez, and S. N. Zhang, editors, *Feeding Compact Objects: Accretion on All Scales*, volume 290 of *IAU Symposium*, pages 25–28, February 2013.
- [16] T. Waters, D. Proga, R. Dannen, and T. R. Kallman. Synthetic absorption lines for a clumpy medium: a spectral signature for cloud acceleration in AGN? , 467:3160–3171, May 2017.

CURRICULUM VITAE

Graduate College
University of Nevada, Las Vegas

Randall Cody Dannen
randall.dannen@gmail.com

Degrees:

Bachelor of Science - Physics, May 2016
University of Nevada, Las Vegas
Bachelor of Science - Mathematics, May 2016
University of Nevada, Las Vegas

Thesis Title:

Force Multiplier Calculations for X-ray Binaries and Galactic Nuclei

Thesis Examination Committee:

Chairperson, Daniel Proga, Ph.D.
Committee Member, Zhaohuan Zhu, Ph.D.
Committee Member, Stephen Lepp, Ph.D.
Graduate Faculty Representative, Evangelos Yfantis, Ph.D.

Honors & Awards:

UNLV Society of Physics Students President, Fall - Spring 2016

Publications:

Dyda, Dannen, Waters, & Proga, Irradiation of astrophysical objects - SED and flux effects on thermally driven winds,
(MNRAS Accepted (2017), arXiv:1610.04292)
Waters, Proga, Dannen, & Kallman, Synthetic absorption lines for a clumpy medium: spectral signature for cloud acceleration in AGN?,
(MNRAS Accepted (2017), arXiv:1611.00407)